"US/DOE Patent Clearance IS NOT REQUIRED prior to the publication of this document."

DOE/PC/89776--T6

9th QUARTERLY PROJECT STATUS REPORT

Project Title: Effects of Calcium Magnesium Acetate on the Combustion of Coal-Water Slurries

DOE/PC/89776--T6

DE92 008701

DOE Grant #: DE-FG22-89PC89776

Principal Investigator: Yiannis A. Levendis

Project Performance Period: 1 September 1991 - 30 November 1991

Project Objectives:

The general objective of the project is to investigate the combustion behavior of single and multiple Coal-Water Fuel (CWF) particles burning at high temperature environments. Both uncatalyzed as well as catalyzed CWF drops with Calcium Magnesium Acetate (CMA) catalyst will be studied. Emphasis will also be given in the effects of CMA on the sulfur capture during combustion. To help achieve these objectives the following project tasks were carried over this 9*th* three-month period.

Project Tasks:

Work on three major tasks was conducted over this period: **(1)** Final results on the pyrometer calibration using the NIST lamp and the newly constructed metal melting equipment. **(2)** Pyrometric observations on the water evaporation period of CWF droplets. And **(3)** Pyrometric time-temperature profiles of burning CWF particles.

CALIBRATION OF THE PYROMETER. WITH THE NIST TUNGSTEN LAMP AND MELTING METALS.

Two different techniques for calibrating the three-color pyrometer were implemented: (i) the NIST tungsten gas lamp and (ii) heating pure metal wires to their melting point. Given the constraints of the present furnace design, the calibration devices were placed outside the furnace, at the bottom. This way the source could be better defined, easily adjusted, and spurious radiation arising from furnace wall reflections on the source could

DISCLAIMER

be minimized.

The gas-filled tungsten-strip lamp was purchased from the National Institute for Standards & Technology (NIST)[39]. The lamp was pre-calibrated at NIST at four different wavelengths, i.e. 0.65, 0.80, 0.975 and 1.20 μm at two apparent temperatures, T_a of 1800 and 2200 K. In this temperature region the lamp's true (actual) temperature, T, can be deduced from Wien's law by accounting for the emissivity of tungsten at any given wavelength:

$$\frac{c_1}{\lambda^5}\exp\left(\frac{-c_2}{\lambda T_a}\right) = \epsilon_\lambda \frac{c_1}{\lambda^5}\exp\left(\frac{-c_2}{\lambda T}\right) \tag{1}$$

thus

$$T = \left(\frac{\lambda}{c_2}\ln\epsilon_\lambda + \frac{1}{T_a}\right)^{-1} \tag{2}$$

Values for the emissivity of tungsten as a function of temperature and wavelength are taken from DeVos.

The lamp was mounted in the upright position below the furnace. A silver-coated mirror (*Newport*) with a rather flat reflectivity (97±2%) over the wavelength of interest, was used to direct the light at a right angle to the collimating lens at the top of the furnace, Fig. 1. Between the lamp and the mirror two pinholes (0.5mm and 1.2mm) were placed in series, spaced 1.5 cm apart, to define the width of the view field. Thus, only a small portion of the tungsten filament, the target area during the NIST pre-calibration of the lamp, was viewed. The lamp and the pinholes were rigidly fastened on a mount which allowed rotation around the centerline of the lamp to permit alignment and testing, before directing the light to the mirror. Finally, a mechanical iris-diaphragm (shutter) was inserted between the pinhole assembly and the mirror. This provided for a baseline when the shutter was closed, and a signal that triggered the data acquisition routine when the shutter was open, Fig. 2.

The lamp was powered by a (*Kikusui*) regulated power supply controlled by a (*Keithley*) 230 programmable voltage source. A typical lamp calibration signal recorded with the three-color pyrometer is shown in Fig. 2; average intensities were computed when the signals reached steady state, the ratios of these average intensities were then calculated and the experiment was repeated for several filament temperatures. The results are shown in Figs. 3 a, b, c, where the logarithm of the ratio of signals at any two wavelengths, corrected for the emissivity of tungsten, $\ln\frac{(S_{\lambda_1}/\epsilon_{\lambda_1})}{(S_{\lambda_2}/\epsilon_{\lambda_2})}$, is plotted versus $1/T$. The slope of the best-fit straight line represents the quantity $c_2\left(\frac{1}{\lambda_2}-\frac{1}{\lambda_1}\right)$ and the intercept is the logarithm of the instrument constant $C_{\lambda_1\lambda_2}$. The slope can also be calculated theoretically. Thus, the

calibration validity can be checked by comparing the theoretical and experimental slopes.

Calibration was also performed observing thin metal wires heated to their melting point. It has been shown elsewhere[1], that the radiance temperatures of metals at their melting points are very reliable secondary calibration sources, since constancy and reproducibility are exhibited irrespective of either the surface conditions of the specimen or the operating parameters. Indeed, excellent reproducibility was found in this study as well. The metals used herein (and their respective melting points) were tungsten (3683 K), platinum (2043 K) and copper (1356 K). A special apparatus was constructed for this purpose, Fig. 1 and 4, and was positioned directly below the furnace. A slender metallic wire (100μm in diameter) was clamped between two cables connected to a large capacitor. A capacitance discharge at an optimum voltage setting caused a large current ($i = CdV/dt$) to flow through the wire, which overheated and melted. The two ends of the wire were masked and the middle portion was viewed through a small slot in order to block radiation from the cooler ends of the wire. Intensity profiles and their respective ratios, plotted against time, are shown in Figs. 5 a,b,c, for tungsten, platinum and copper, respectively. The flat portions of the intensity ratio profiles correspond to the phase change that takes place at constant temperature when metals transform from solid to liquid. These results are also plotted in Figs. 4 a,b,c along with the lamp calibration results. However, to incorporate emissivity corrections at the melting temperatures of the metals, emissivity data at the three wavelengths of this study was needed. For tungsten such data were obtained by extrapolation from the results of DeVos. Emissivity data for platinum and copper was found at the 0.65 μm wavelength only. Thus, using all the available emissivity data and the known melting temperatures of the metals, and then fitting the theoretically calculated slopes for the other two wavelengths the metal calibration lines of Fig. 4 were obtained. With this technique the emissivities of platinum and copper at 0.810 and 0.998 μm were estimated, see Table I:

[1]Cezairliyan, A., Miller, A. P., Righini, F. and Rosso, A. (1982). "Radiance Temperature of Metals at their Melting Points as Possible High Temperature Secondary Reference Points." *Temperature, Its Measurement and Control in Science and Industry*, American Institute of Physics, 379.

TABLE I

Emissivity at the melting point temperatures of metals.

Metal	$\lambda = 0.640\mu$m	$\lambda = 0.810\mu$m	$\lambda = 0.998\mu$m
Tungsten	0.412*	0.381*	0.362*
Platinum	0.381†	0.300	0.250
Copper	0.161†	0.112	0.087

*extrapolated from De Vos, J. C. (1954). "A New Determination of the Emissivity of Tungsten Ribbon" *Physica* **XX**, 690.

† from Gubareff, G.G., Jansen, J.E. and Torborg, R.H. "Review of the Thermal Radiation Property Values for Metals and other Materials." Honeywell Research Center Report, Mineapolis, 1960.

The rest estimated from this study with maximum uncertainty of ± 0.01.

The theoretical slopes of any two-wavelength pairs ($c_2/T(1/\lambda_2 - 1\lambda_1)$) are also plotted in Fig. 4 for comparison. From the same figure it can be seen that the discrepancy between the two calibration lines (lamp and melting metals) ranges from 50 K to 100 K at the low and the high temperature region, respectively, for the three two-wavelength combinations. The lamp calibration was used for analyzing the results of the present study.

Two problem areas should be discussed here: (a) Thick cables and a heavy duty mogul-type socket should be used with such a high current lamp(40 Amps), since slight overheating of the cables and connections causes filament temperature drifts and erroneous readings. Furthermore, the "sense" wires of the power supply should be connected all the way to the socket terminals. (b) For the calibration with melting metals, notching of the wires to induce localized melting was found undesirable since it produced sparks and excessively high temperature readings. This might be due to formation of a high temperature arc.

PYROMETRIC OBSERVATIONS ON THE WATER EVAPORATION PERIOD OF CWF DROPS.

The time for evaporation of the liquid portion of the CWF droplet has been determined earlier in this study (see Reports 3 and 4) for different coal loadings and different solvents such as water, acetone and ethanol. To experimentally determine this time in our system a slight modification was done to the currently used drop generator. This generator uses a mechanically actuated plunger to eject a drop, Fig. 6, as described in an earlier report. A light source and a photosensor were connected across the moving stem of the solenoid actuator, Fig. 6, and every time the stem moved downwards a voltage signal was created,

in this case 4V. An extra available channel in the A/D board was utilized for recording this signal. The frequency of acquisition in each channel was effectively reduced from 33 kHz to 25 kHz. The wall temperature of the furnace for these experiments was maintained at 1500 K. The flow of air through the injector was 0.1 lpm and the furnace flow was an additional 2.0 lpm.

The droplets were generated at the top of the injector tube and, therefore, traversed the cold environment of the injector before it entered the hot radiation zone. Subsequently, it heated up, ignited and burned. Temperature-time profiles for three different droplets; two of them having diameters $\approx 250\mu$m and the third $\approx 500\mu$m are shown in Fig. 7. The recorded time for evaporation and subsequent particle heat-up was around 600 msec (time is counted from the middle of the spike and start of solid agglomerate combustion), see Table II. Only one of the intensity signals, at 0.65μm, is represented on the plot. The signals were recorded with logarithmic amplifiers, which are inverting in nature, so any increase in temperature and/or light intensity will be presented by a decrease in voltage signal. From the signal trace we can see an initial peak and then a steadily decreasing signal. The initial peak is related to the release and combustion of the volatiles; the second stage represents the combustion of the char residue. More on the combustion behavior of slurries will be given in the next section. Now, the water evaporation time can be contrasted with that calculated numerically by Cumper *et al.* for 250μm size CWS drops. It can be calculated that 250μm size droplets need $\approx$680 ms for complete evaporation if injected from the same hight as in the experiments. This is the same as the experimentally observed time. Of cource there some considerable uncertainty in the initial size of the drops generated by this device, and the actual mechanism of evaporation of water at the presence of the coal slurry, (i.e. formation of a shell with water trapped inside, swelling, further water evaporation, etc.) is different that the "water shell and carbon core" model that the calculation assumed. Furthermore, it is possible that leaching organics from the coal tars to the water alter the properties of the latter to a degree. Nevertheless the agreement was very good indicating that the evaporation behavior of CWF droplets can be approximated by a simple model.

PYROMETRIC TIME-TEMPERATURE PROFILES OF BURNING CWF PARTICLES.

These studies were conducted with dried CWF particles. The reason for this is given

in the following. Since the CWF droplets obtained from the droplet generator were not of accurately controlled and repeatable size, the initial diameter of the dry CWF agglomerated particle was not known. This impaired the accuracy of subsequent studies on the burning CWF particle. Hence the droplet generator was used in a separate reactor to produce dried agglomerates, as described in Quarterly Report #7. The temperature in that reactor was kept at the minimum required for complete water evaporation (600°C) and the atmosphere was nitrogen. An SEM micrograph of such an CWF agglomerated particle is shown in Fig. 8. The size of these agglomerate particles was first measured under a microscope and then were dropped into the high temperature furnace, through the drop for dry injection, by means of a bevel-shaped needle.

Six different representative profiles of burning CWF particles are given in Figs. 9-15. In all plots the intensity-time profiles are shown for all three wavelengths of the pyrometer, as well as the temperature-time profiles. In Fig. 9 the associated relative particle size is also plotted. This was obtained as described in the following:

Determination of Change in Particle Size. In principle, the multi-color optical pyrometry technique has the potential of determining the change in radiating source area. Along the particle trajectory let the signal strengths be S and S_r where the particle temperatures are T and T_r (r represents any chosen reference point). The signal strength is proportional both to $e^{-c_2/\lambda T}$ (if the temperature is not too high to invalidate the Wien approximation) and to $\epsilon_\lambda A_c/L^2$, where A_c is the projected radiative area*[2] of the particle and L is the distance from the sensor. The signal ratio at the two points is then

$$\frac{S_\lambda}{S_{\lambda,r}} = \frac{A_c}{A_{c,r}} \frac{\epsilon_\lambda}{\epsilon_{\lambda,r}} \left(\frac{L_r}{L}\right)^2 e^{\frac{c_2}{\lambda}\left(\frac{1}{T_r}-\frac{1}{T}\right)} \tag{3}$$

Since the present study employs low-velocity laminar gas flow in the combustion experiments, the distance traveled by a particle during combustion is a very small fraction of L, and $(L_r/L)^2$ may be assumed 1. In addition, carbon emissivity varies little enough with temperature[43,44] to justify setting $\epsilon_\lambda/\epsilon_{\lambda,r} = 1$. Then the area ratio is given by

$$\frac{A_c}{A_{c,r}} = \frac{S_\lambda}{S_{\lambda,r}} e^{\frac{c_2}{\lambda}\left(\frac{1}{T}-\frac{1}{T_r}\right)}, \tag{4}$$

Any wavelength may of course be used for evaluating the signal ratio; T and T_r come from wavelength pairing of signals.

[2]Corresponding to the portion of the particle that has ignited.[30]

Discussion of the Results All Figures 9-15 show single dried CWF agglomerate traces burning in air at 1500 K; the sizes ranged from 195 to 495μ as noted in the figures. The traces in Figs. 9 and 10 were recorded with linear amplification while the rest with logarithmic amplification and are thus inverted. There is a clear hump at the beginning of the signal which is associated with volatile release and simultaneous combustion. This lasts for a fraction of the overall burntime, in the neighborhood of 20%, see Table II.

Combustion of the volatiles takes place at ≈2250K and combustion of char at ≈2000K. For the former case, the emissivity of soot has not been accounted for yet. The temperature profile during the agglomerate combustion is rather flat. It is interesting to note that at the end of the period associated with the combustion of volatiles there is a low luminosity region where the char agglomerate ignites. Thus, it appears that the char ignites at the end, and not during, the combustion of volatiles. Such behavior will be investigated further by high speed cinematography.

To calculate the change in particle diameter, using the equations above, the reference point was taken at the point in time where the agglomerate was heating up to its near-steady state combustion temperature after ignition, Fig. 9. At this point the agglomerate was assumed to have a diameter equal to that observed under the microscope corrected by a swelling factor. Swelling was studied earlier (see Report #7). A swelling factor of 1.12 was assumed here for all particles. The relative diameter plot shows that the size of the agglomerate decreases continuously throughout combustion. It is important to note that the same technique can be used to estimate the size of the volatile flame in the first region of the combustion. In the case depicted in Fig. 9 the size of the 1.4 times the initial diameter of the agglomerate. More results need to be analyzed to examine trends.

PRESENT WORK and FUTURE PLANS At present, work is being conducted on (a) Pyrometric observations on burning single CWF particles with and without CMA. (b) Pyrometric observations on burning single CWF particles with and without CMA, from two different coal grids. (c) Reaction rate calculations - selection and development of models. And (d) SO_x capture experiments with dry-spraying various sorbents.

12/20/91

TABLE II

	File.	Size (mm)	Time total (msec)	Time volatile (msec)	Time char (msec)	Time theory (msec) (*2)	Temp volatile (K) (%)	Temp char (K) (%)	
In air T_∞ = 1500 K main flow = 2.0 lpm by flow = 0.1 lpm	linair7φ1.dat	195	146	20	126	230	2375	2200	
	a2.dat	270	320	60	260	455	2250	2050	
	a4 dat	300	324	74	250	580	2250	1900	
	a3 dat	330	360	71	289	685	2175	2000	
	a5.dat	420	381	100	281	1115	2300	2000	
	⇒ *1 slurry dat	495	587	72	515	1500	2425	2150	
Fourth channel in air T_∞ = 1500 K main flow = 2.0 lpm by flow = 0.1 lpm temp: from middle of spike									Evaporation (msec)
	A1		130	37	93		2250	2050	655
	A2		155					2350	565
	A3		505	105	400		2275	2050	570

*1 also on photographs; *2 with ρ (density) = 600 kg/m³

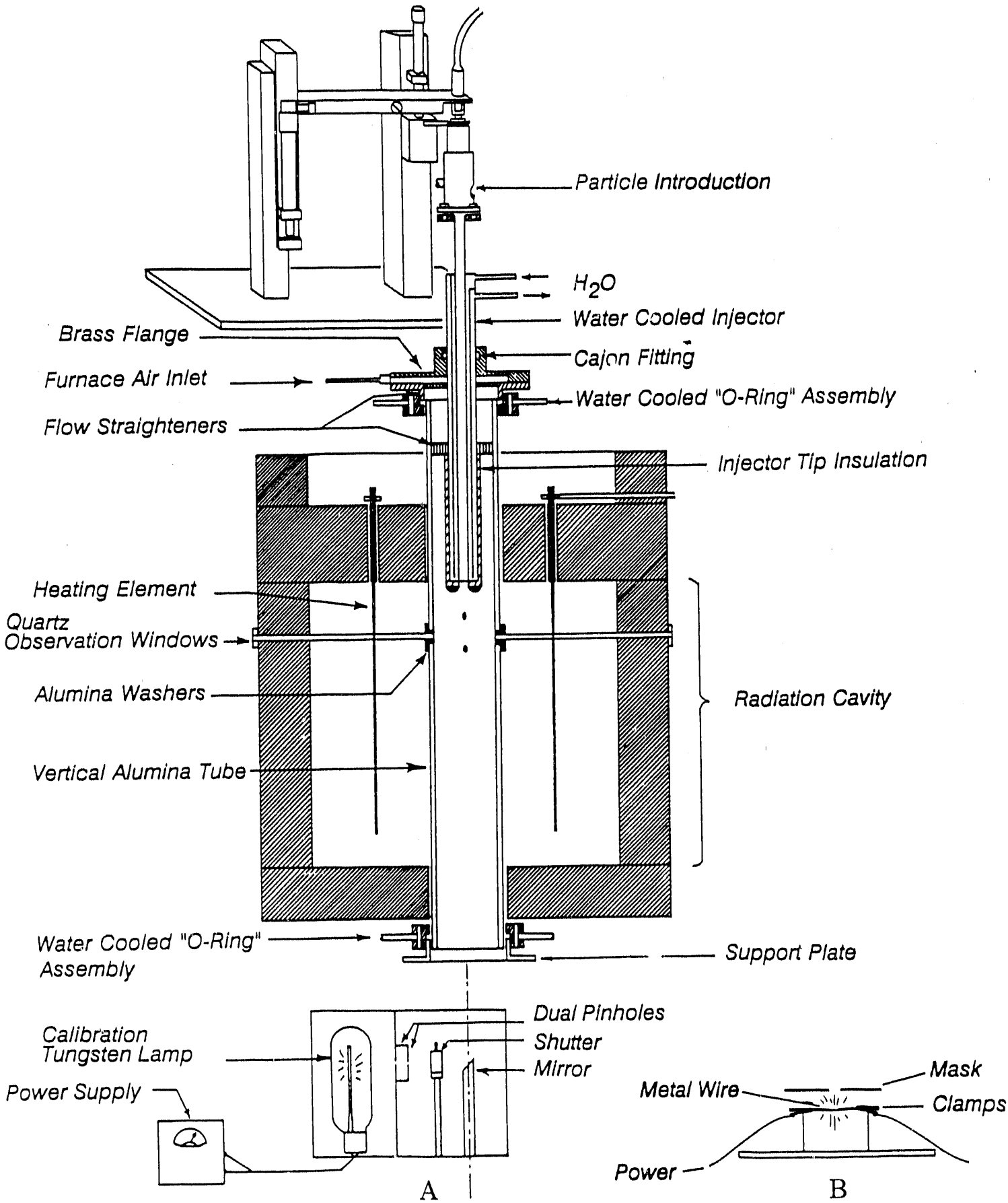

1. Schematic of the laminar flow furnace, monitoring optics and calibration devices (a) Calibration setup using a NIST tungsten lamp and (b) Calibration setup using the melting temperature of different metals

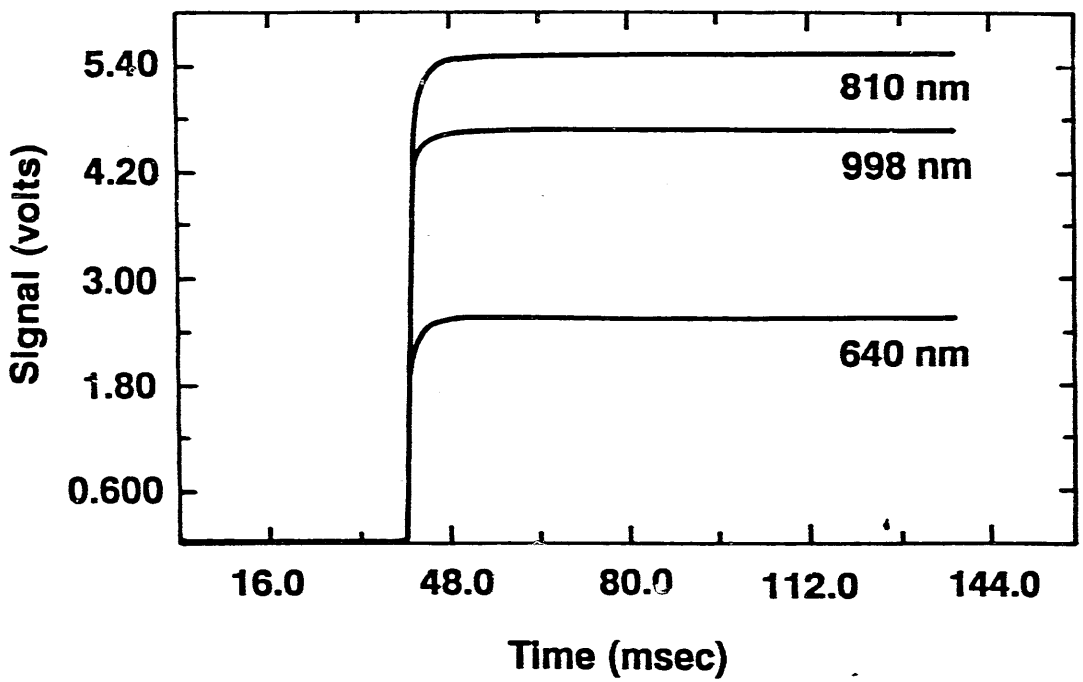

2. NIST lamp calibration signal as recorded by the three-color pyrometer; the true lamp temperature was 2100 K. The profile was recorded with the medium bandwidth filters and linear amplification.

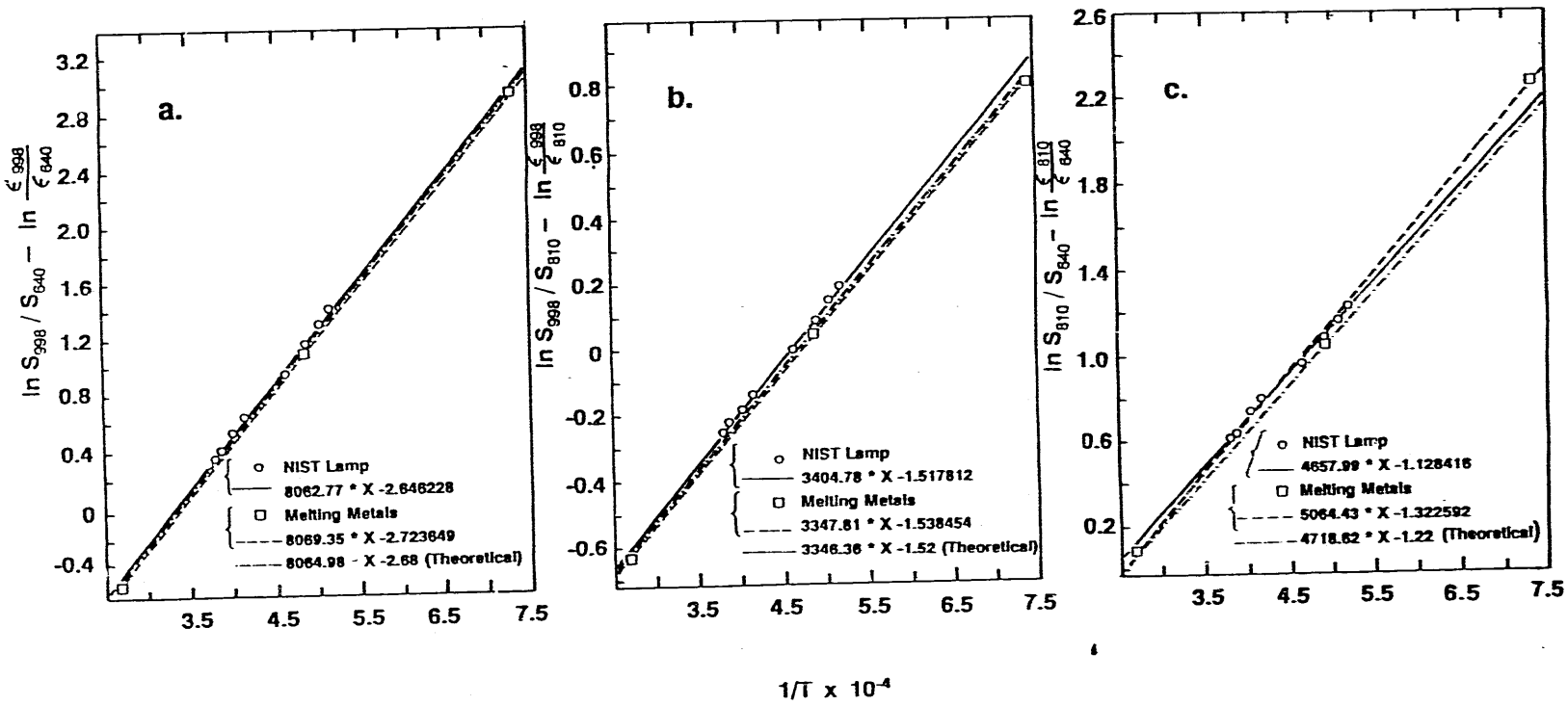

3. Semi-logarithmic calibration plots at the different color ratios of the three-color pyrometer, (a) 998/810 nm, (b) 998/640 nm, and (c) 810/640 nm. Both the NIST lamp calibration and the calibration using the melting point of metal wires are plotted.

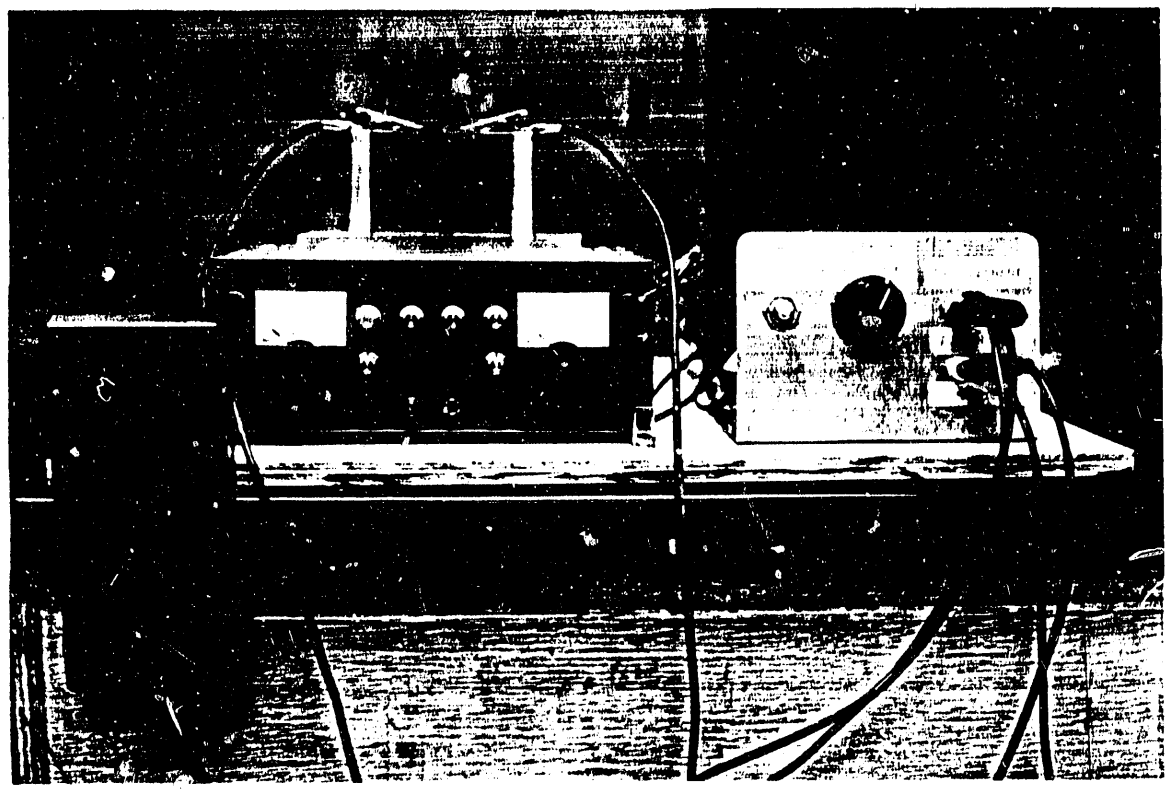

Figure 4.2.1(a) Melting Metal Assembly

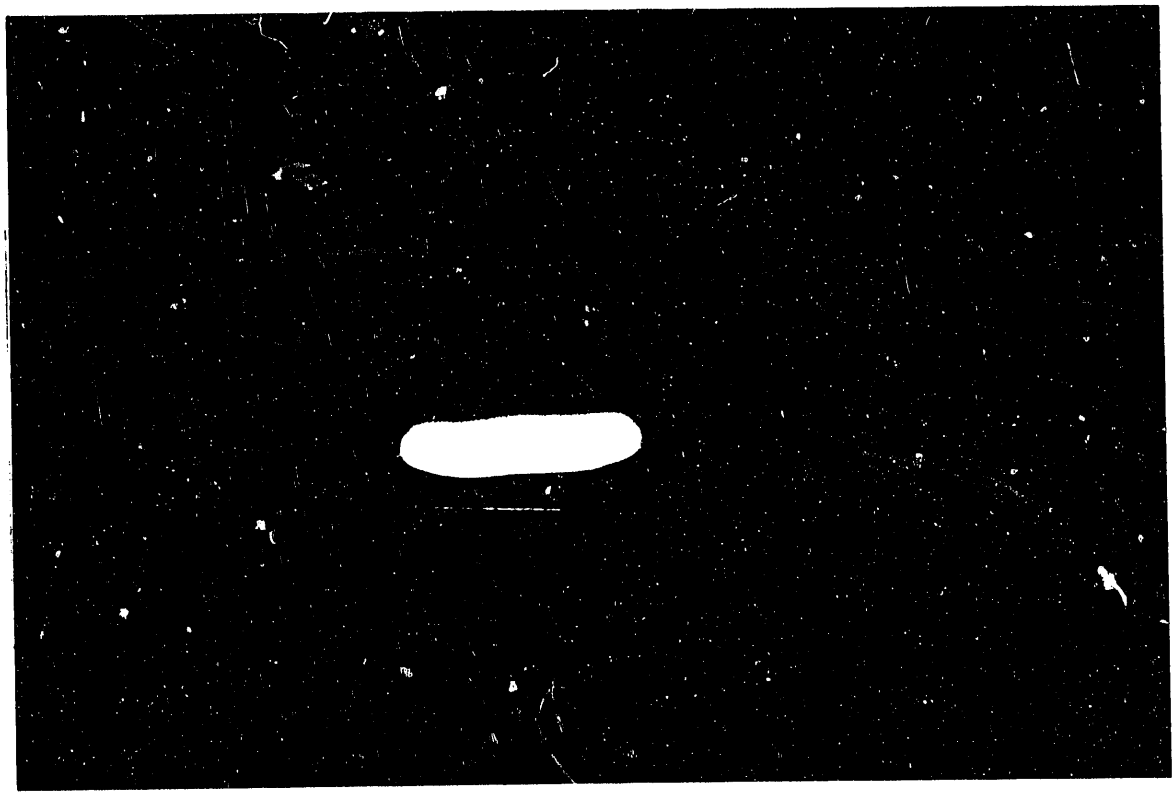

Figure 4.2.1(b) A Melting Wire

5. Intensity signals (top row) and intensity ratios (bottom row) as recorded by the three-color pyrometer, with the medium band-width filters and linear amplification. (a) tungsten, (b) platinum and (c) copper.

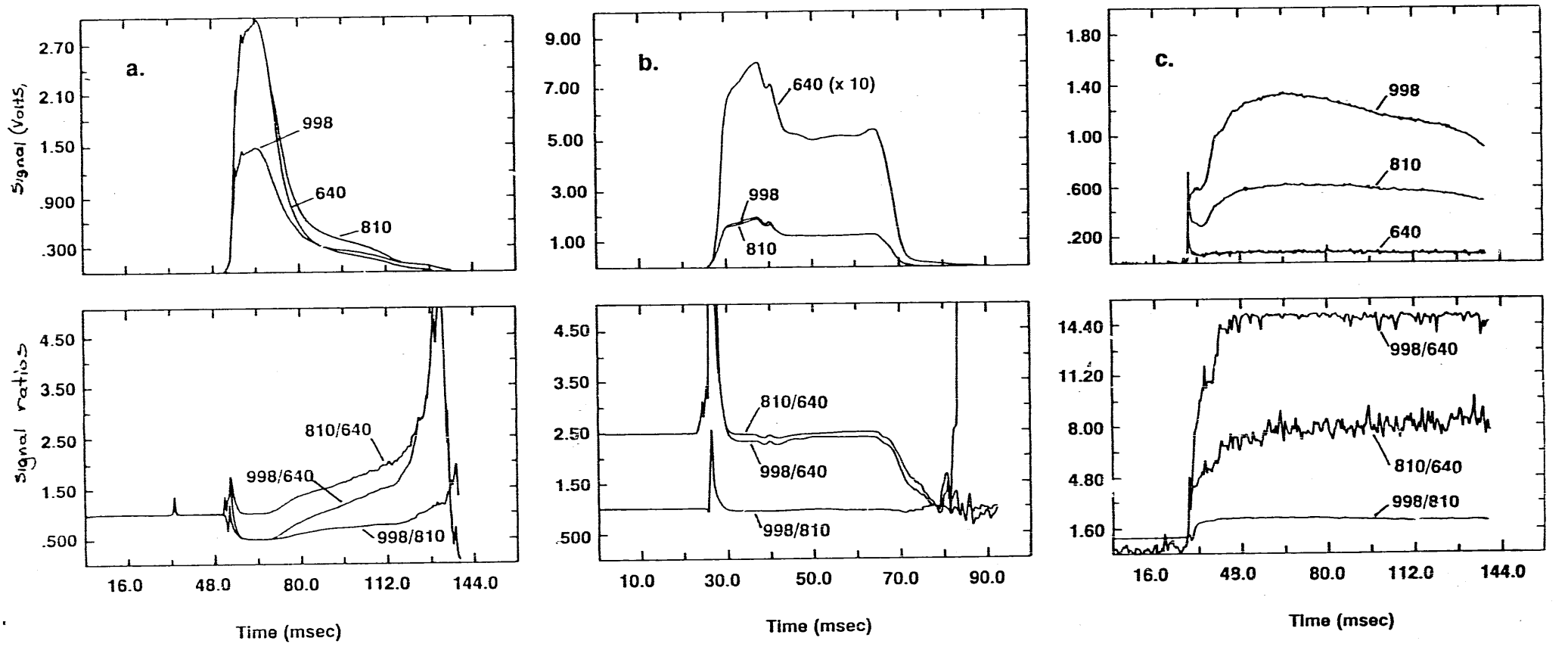

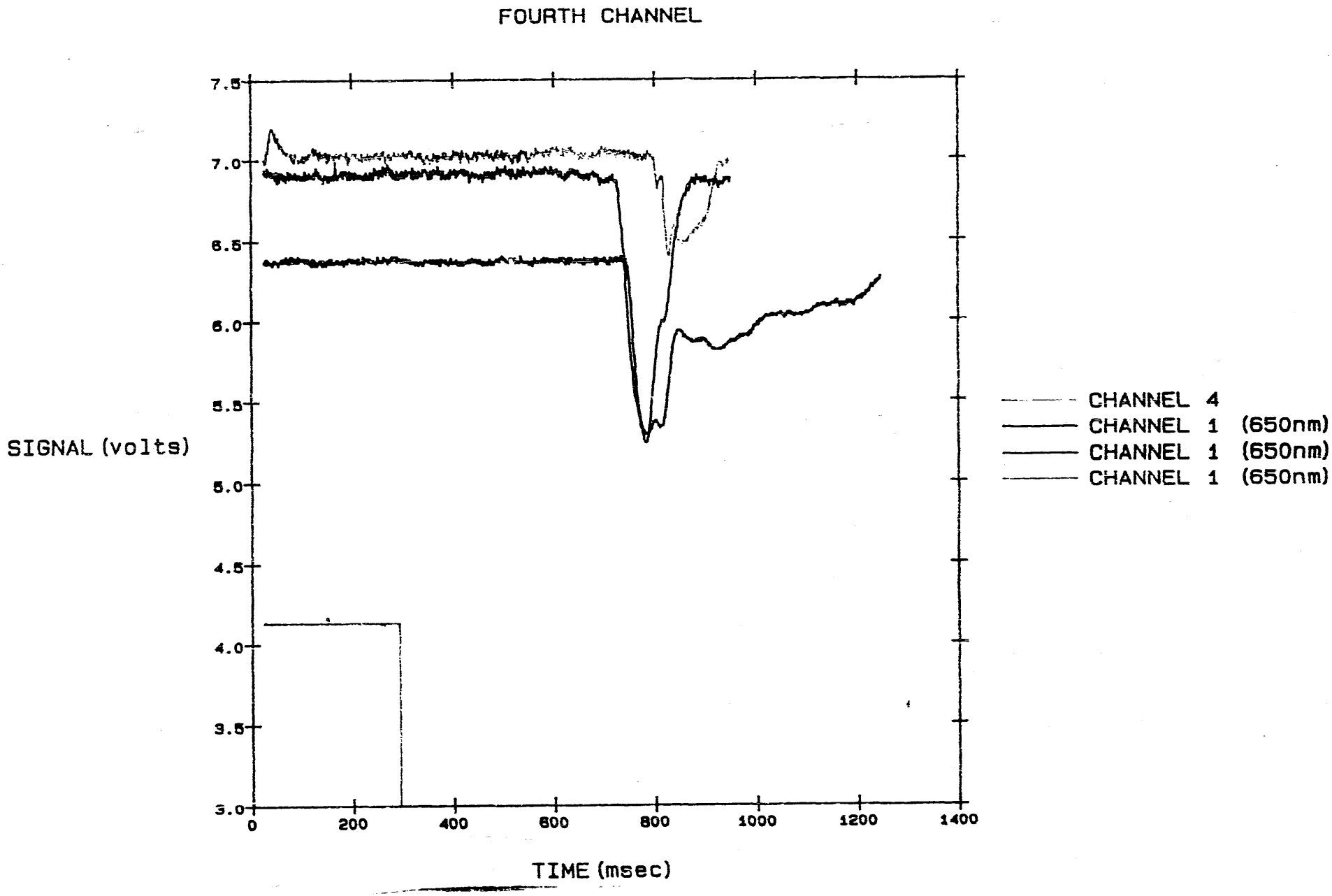

7. Intensity signals for burning three superimposed CWF droplets in air at a gas temperature of 1400 K as recorded by the three-color pyrometer, with the medium bandwidth filters and linear amplification. The forth signal is from the photocell and records the beginning of injection, marked at the middle of the signal.

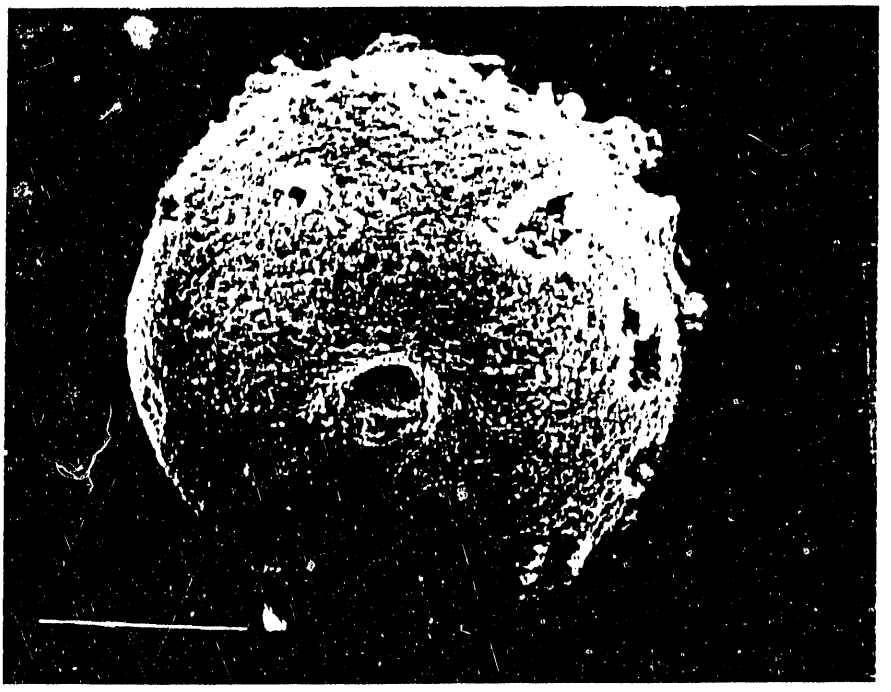

Figure 3.3.1(a) Magnification=300

Figure 8. Dry slurry agglomerate ; dia=250 μm ; Magnification = 2000

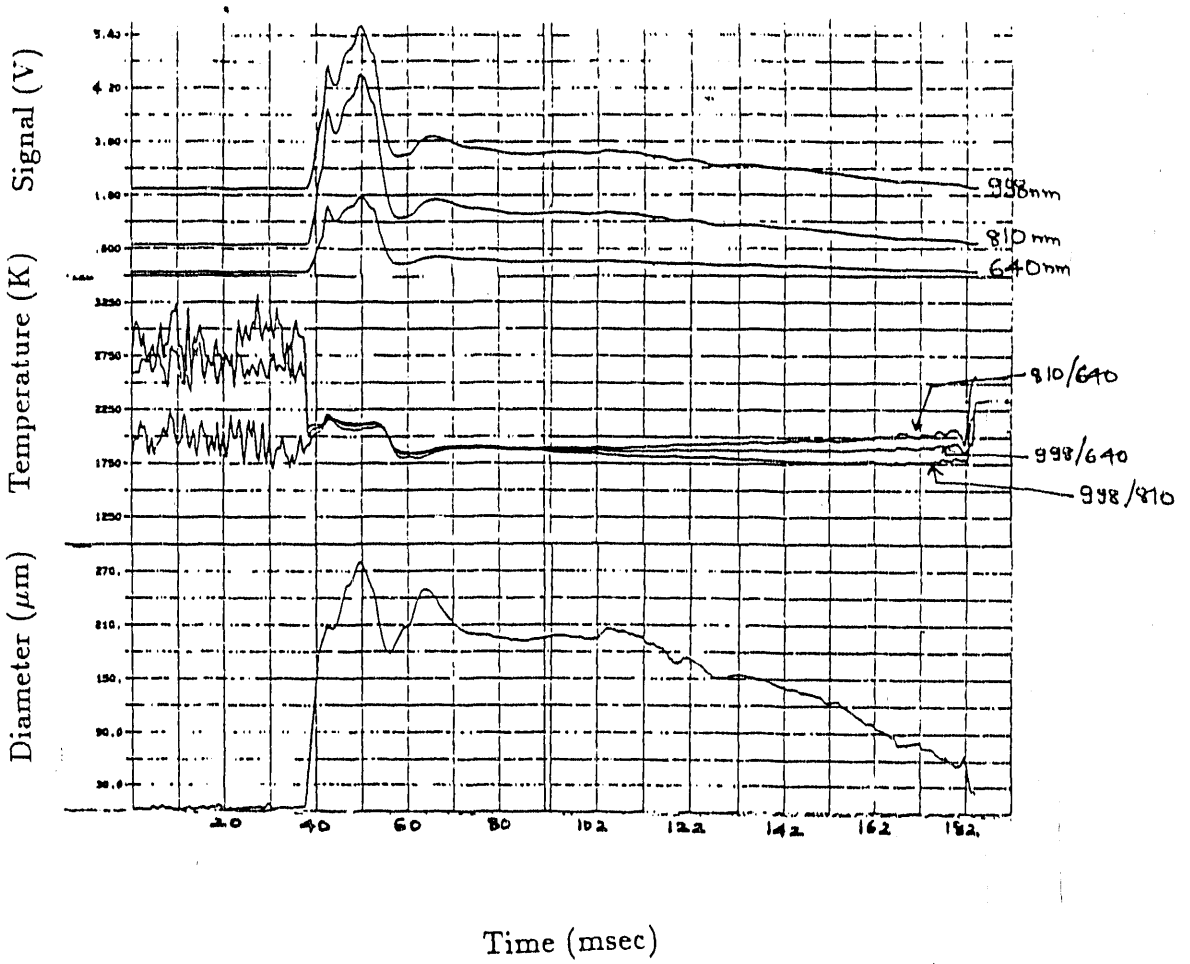

9. Intensity signals (top row), temperature profiles (middle row) and relative agglomerate diameter (bottom row) for burning CWF agglomerates in air at a gas temperature of 1400 K as recorded by the three-color pyrometer, with the medium band-width filters and linear amplification.

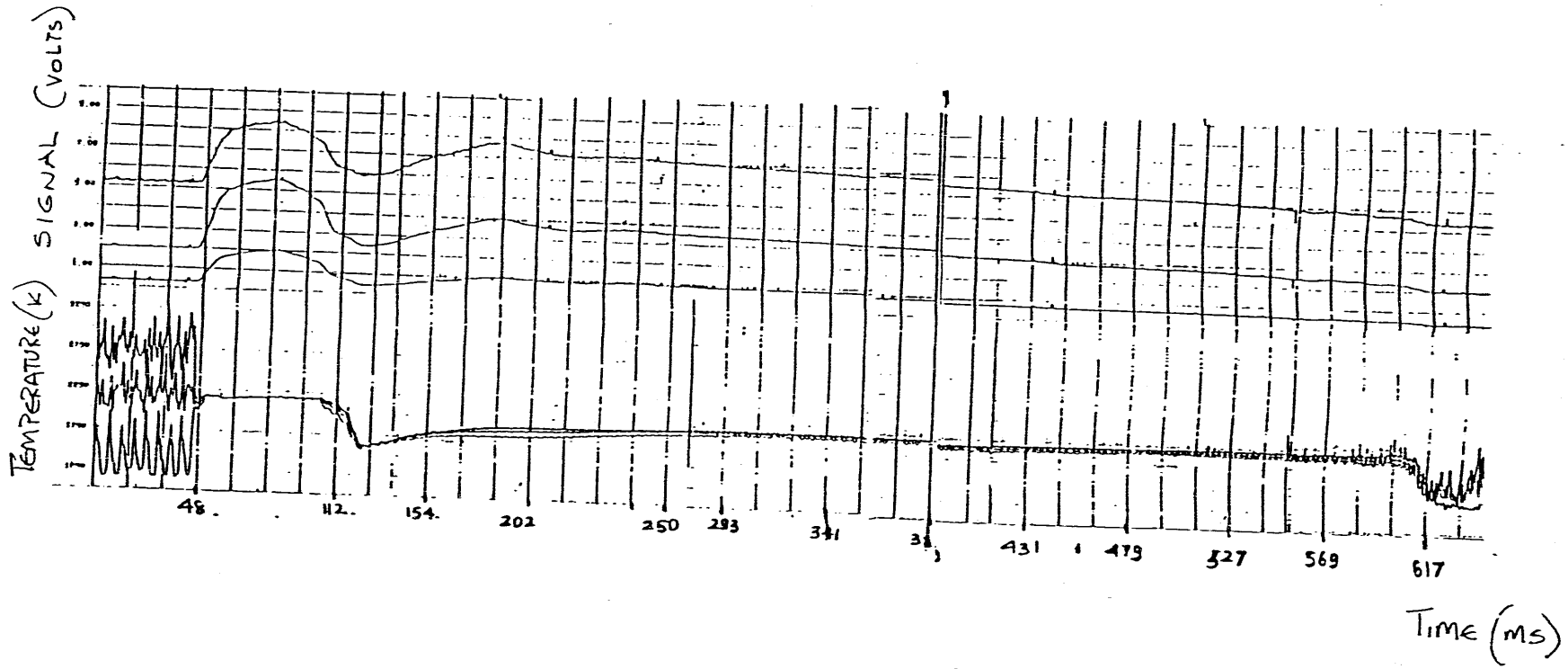

10. Intensity signals (top row) and temperature profiles (bottom row) for burning CWF agglomerates in air at a gas temperature of 1400 K as recorded by the three-color pyrometer, with the medium band-width filters and linear amplification.

$d = 49.5 \mu m$

$T_w = 1500$ K

in air

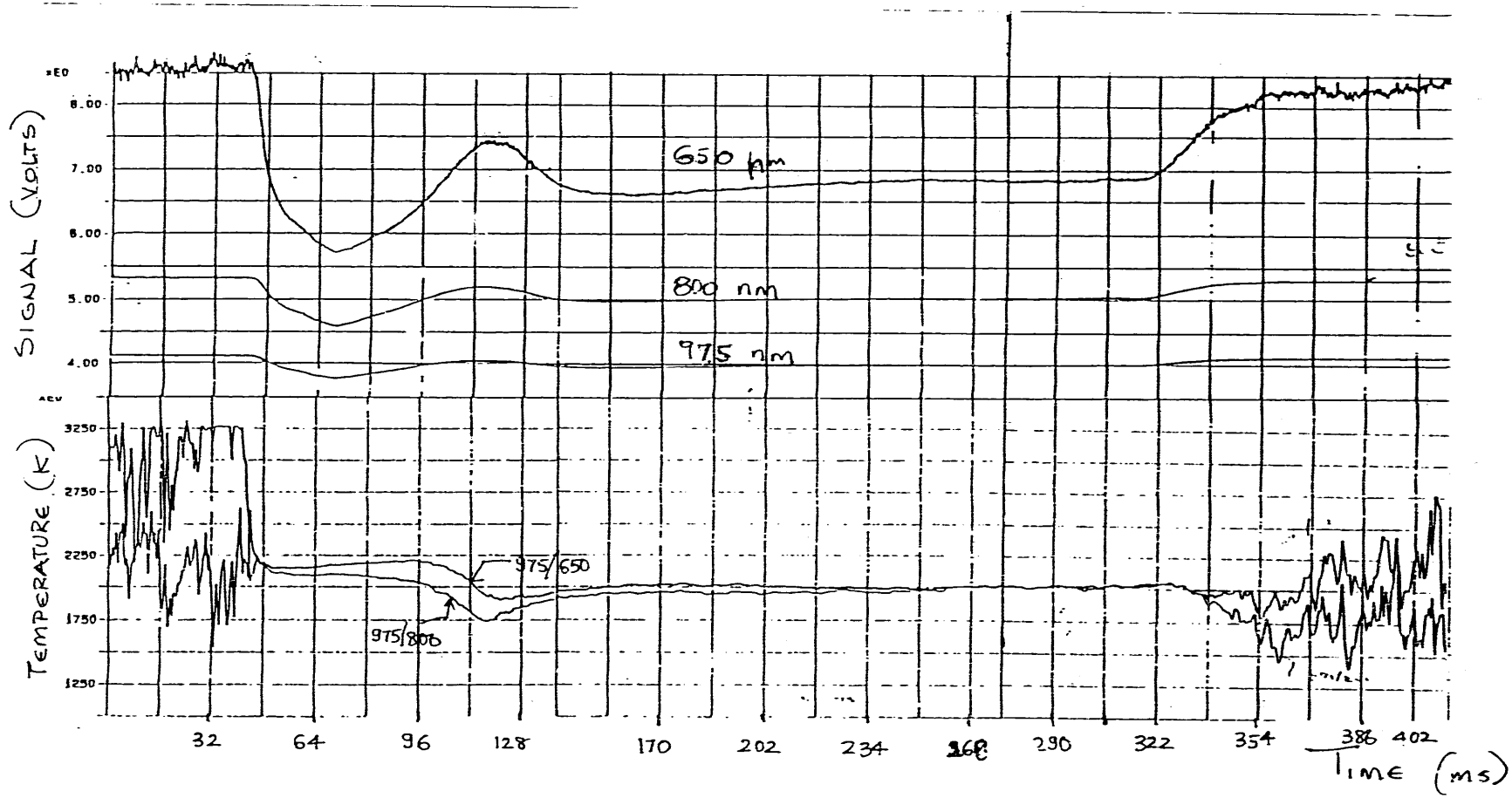

11. Intensity signals (top row) and temperature profiles (bottom row) for burning CWF agglomerates in air at a gas temperature of 1400 K as recorded by the three-color pyrometer, with the medium band-width filters and logarithmic amplification.

a2.dat
d = 270μm
T_w = 1500μm
in air

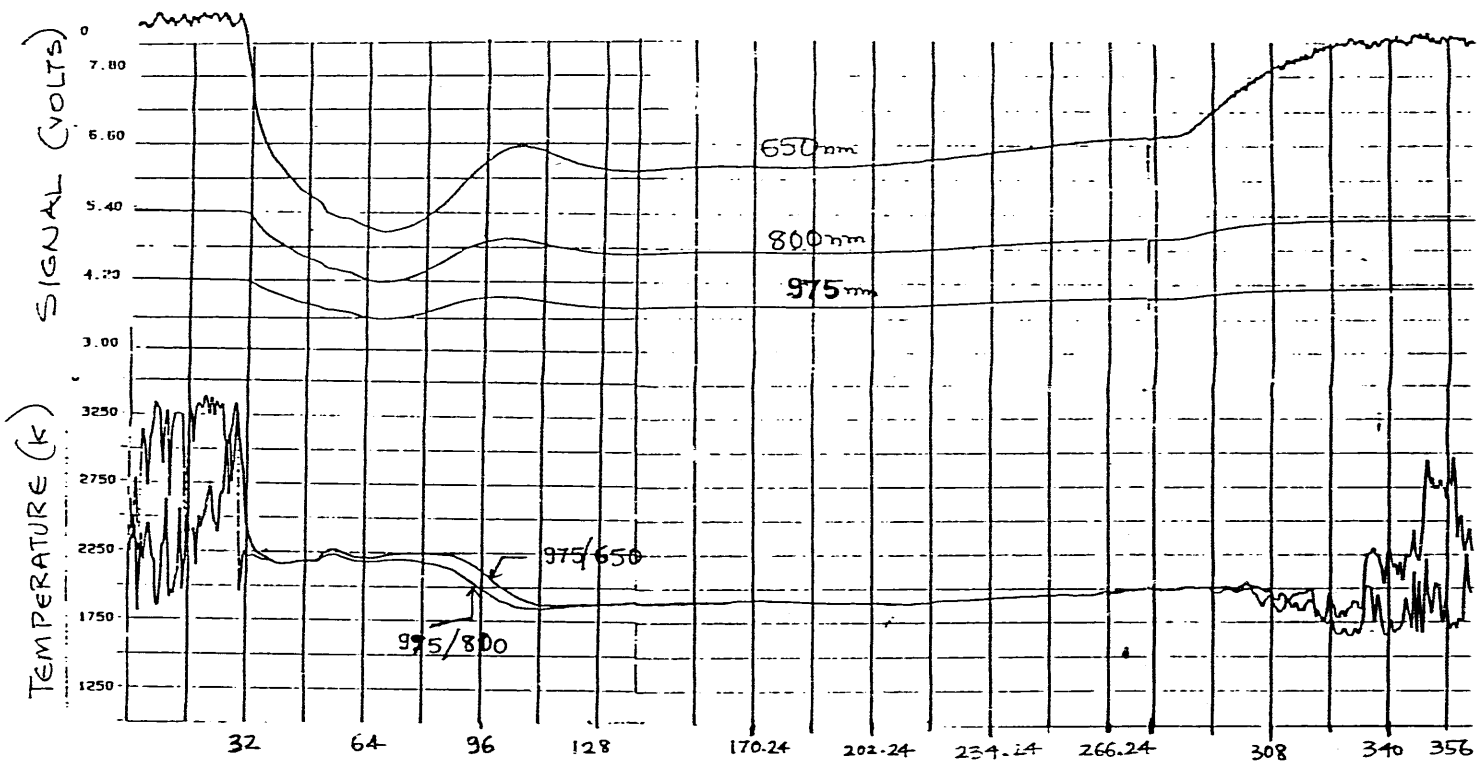

x4.dat
d=300 μm
T_w=1600 μm
in air

12. Intensity signals (top row) and temperature profiles (bottom row) for burning CWF agglomerates in air at a gas temperature of 1400 K as recorded by the three-color pyrometer, with the medium band-width filters and logarithmic amplification.

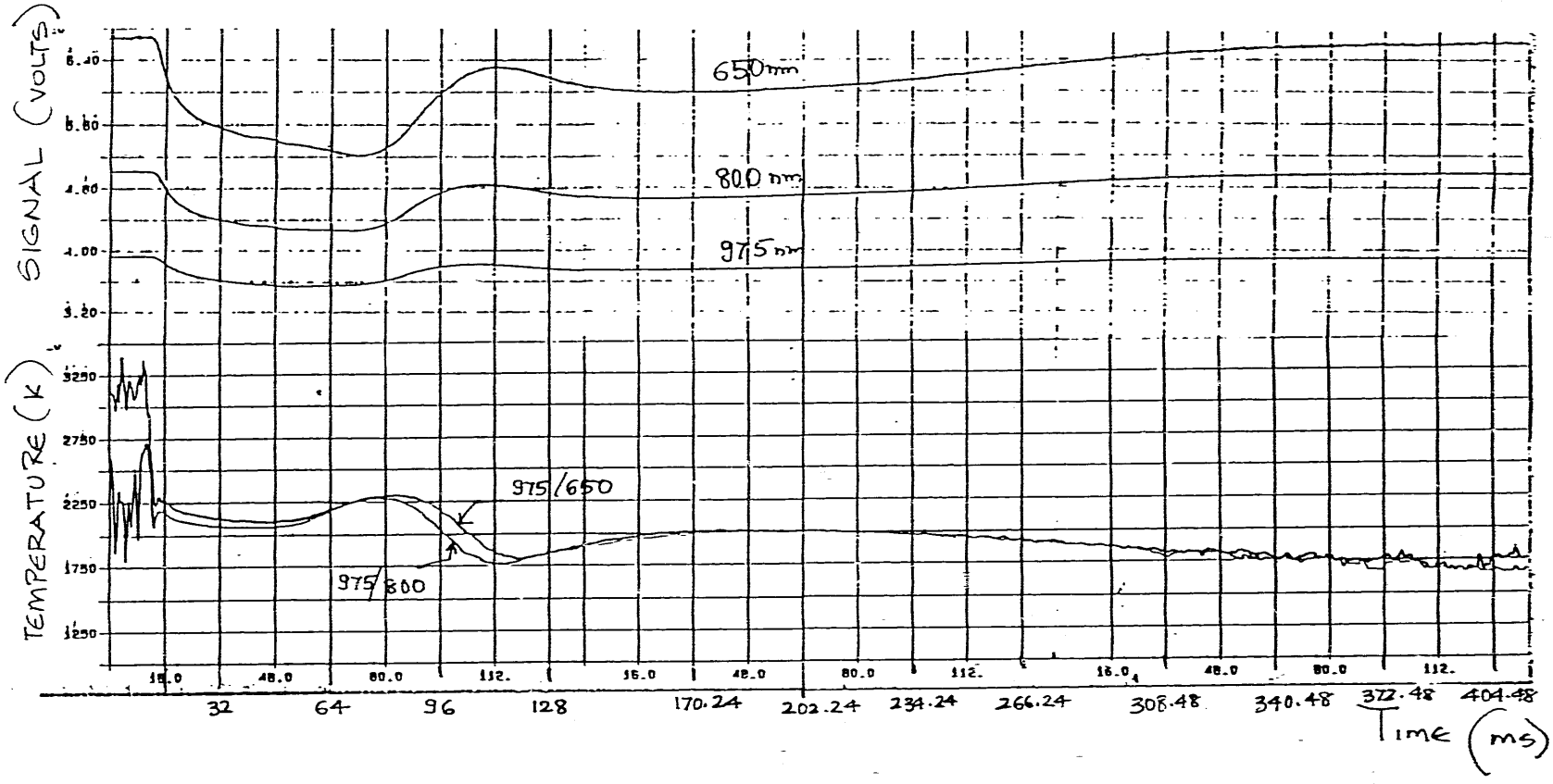

a3 · dat

d = 330μm

T_g = 1500 K

in air

13. Intensity signals (top row) and temperature profiles (bottom row) for burning CWF agglomerates in air at a gas temperature of 1400 K as recorded by the three-color pyrometer, with the medium band-width filters and logarithmic amplification.

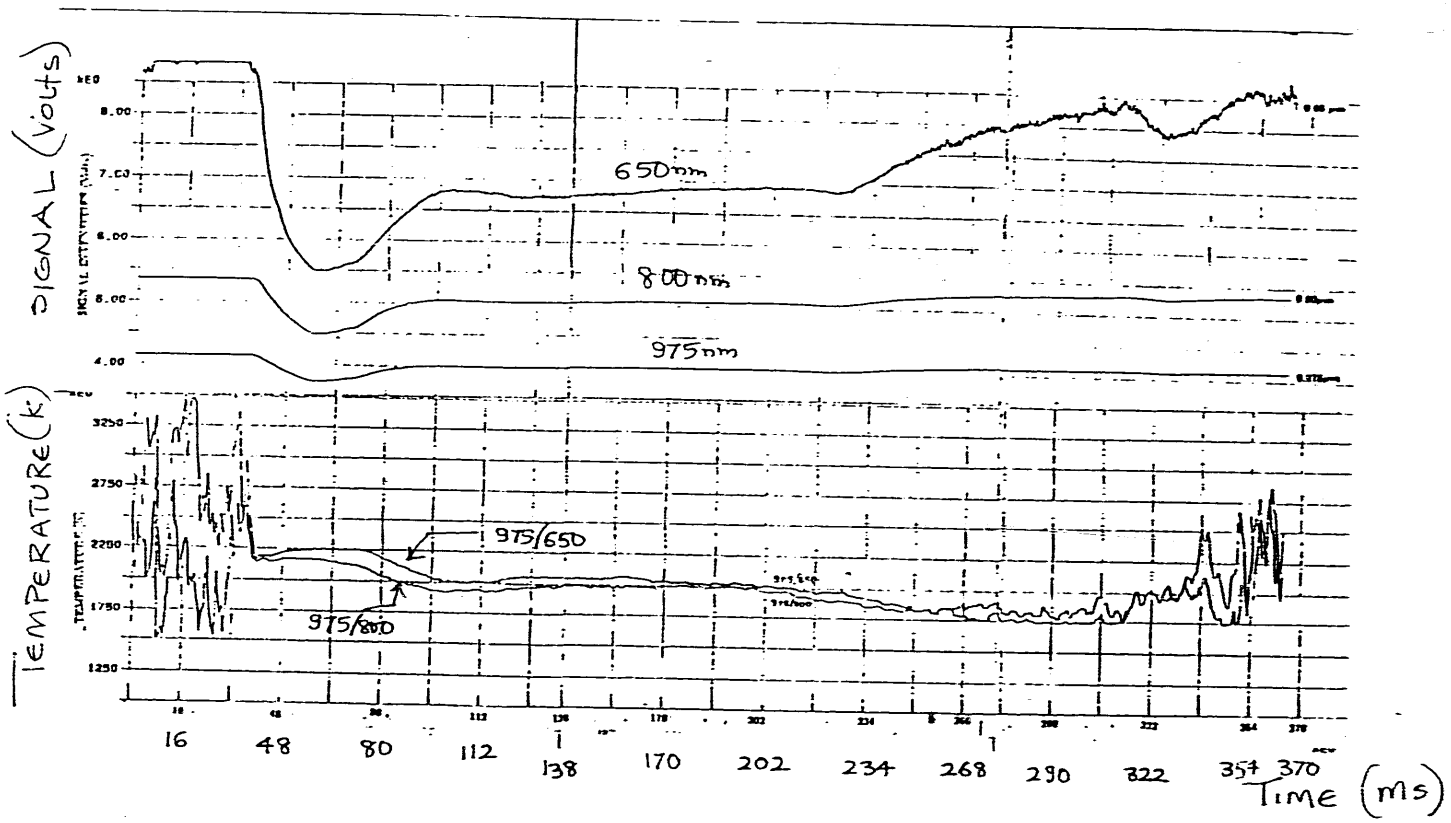

u5.dat

d=420μm

T_w=1500 K

in air.

14. Intensity signals (top row) and temperature profiles (bottom row) for burning CWF agglomerates in air at a gas temperature of 1400 K as recorded by the three-color pyrometer, with the medium band-width filters and logarithmic amplification.

END

DATE FILMED

4/06/92